Energy Harvesting from Lead-free Piezoelectric materials

A dissertation submitted in fulfilment of the requirements for the degree
Of

MASTER OF SCIENCE

In

PHYSICS

Submitted by
Raj Ankit
(301804014)

Under the Guidance of

Dr. Jayant Kolte
Asst. Professor, SPMS

Submitted to:

School of Physics and Materials Science

Thapar Institute of Engineering and Technology, Patiala-147001

July, 2020

DECLARATION

I hereby declare that the work which is presented in dissertation entitled **"Energy harvesting from lead-free piezoelectric material"** being submitted to School of Physics and Material Science, Thapar Institute of Engineering & Technology (Deemed to be University), India is the original work of mine carried out under the guidance of **Dr. Jayant Kolte** during 7 January 2020 to 15 July 2020 and has not submitted previously in the form of manuscript/thesis for publication or for the award of any degree, diploma or similar internship report.

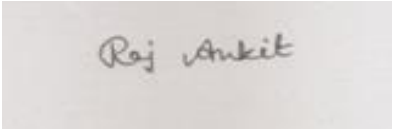

Place: Patiala

Date: 15.07.2020

Raj Ankit

M.Sc. – Physics (2018-20)

Enrolment No :301804014

School of Physics and Material Science

TIET, Patiala

CERTIFICATE

This is to certify that the present research work entitled **"Energy harvesting from lead-free piezoelectric material"** being submitted by Mr. Raj Ankit (Enrolment No: 301804014), School of Physics and Material Science, Thapar Institute of Science and Technology, Patiala is a record of bonafide research carried out by him under my supervision and guidance during 7 January 2020 to 15 July 20120 at), School of Physics and Material Science, Thapar Institute of Science and Technology, Patiala.

Dr. Jayant Kolte

Associate Professor

School of Physics and Material Science,

Thapar Institute of Engineering &
Technology, Patiala (Punjab)

FORWARDED

Prof. O.P. Pandey

Head

School of Physics and Material Science

Thapar Institute of Engineering

& Technology, Patiala – (Punjab)

ACKNOWLEDGEMENT

First of all, I would like to thank to the God, who is the creator of this universe and it is his mercy and blessing to me that this work become possible.

I would like to express my sincere gratitude to my supervisor **Dr. Jayant Kolte** for his unlimited guidance, insight and suggestions throughout the research. I thank him from the bottom of my heart for introducing me to the area of electro ceramics. I thank him for his great patience, constructive criticism and myriad useful suggestions apart from invaluable guidance to me.

I am grateful to **Prof. O.P. Pandey**, Head of School of Physics and Material science (SPMS) for his encouragement and help to carry out the thesis work. I am also indebted to my senior research colleague **Ms Neha Thakur** for her unconditional support and constant motivation whenever needed.

I am very grateful to my dear friends **Rhythm**, **Purnima**, **Sherry**, **Shreya** and **Vandana** who has given me their friendship, put up with my odd hours, and provided me with lifts and practical help.

Last but not the least; I would like to thank my dear parents, my elder brother especially **Manik Chandra Pandey**, without their support it was not possible to come so far.

Raj Ankit
(301804014)

Abstract

Barium calcium zirconate titanate ($Ba_{0.85}Ca_{0.15}Ti_{0.9}Zr_{0.1}O_3$, BCZT) ceramic have been successfully synthesised by sol-gel method. The synthesized powder is calcined at 1000℃ for 3hr, to obtain the single-phase perovskite structure. The flexible nanocomposite films of BCZT/ Polyvinylidene fluoride (PVDF) has been fabricated by solution casting method. The microstructure and the morphology have been studied by SEM. The particle is homogenously dispersed in the PVDF matrix as confirmed by SEM. Formation of the phase and crystallite size is obtained by the X-ray diffraction. The average crystallite size obtained is ~ 26nm.

Table of Contents

List of Figures

List of Tables

Chapter - 1

Energy Harvesting

1.1 Introduction

Governments around the world are looking for ways to boost their economies, with an emphasis on multidisciplinary research. This involves investment that focuses on science, research, and innovation, with development of a number of priority technologies. The governments and legislators will concentrate on delivering affordable and clean energy sources. The growth in the energy sector is constantly under review to ensure new technologies are developed locally.

The better utilisation of energy resources will be just as critical in the few decades as seeking alternative sources of supply. Development of new technologies has become more important because the country's demand of energy keeps on increasing. Traditional technologies can be considered as efficient in meeting the demand, but have a significant negative impact on the environment and resources. The fossil fuels used in conventional technologies are likely to continue for next 30 years, but substantial progress in reducing carbon dioxide emissions has been made. The need for new energy harvesting technologies from the renewable energy source has become important than ever. In the recent past the research in the field of energy harvesting has attracted a lot of attention by generating a low-grade environment friendly energy sources, like environmental vibrations and human power as usable electrical energy. These devices are, therefore can be considered as replacements for primary batteries in low-power electronics.

In this report, energy harvesting systems with a focus on piezoelectric energy harvesting is discussed. This report demonstrates the current progress within piezoelectric energy harvesting and challenges faced within the field.

1.2 What is Energy Harvesting?

The extraction of energy from ambient sources and storing it for the utilisation of different purposes is called an energy harvesting (EH). Researchers are developing techniques for extracting energy from heat and other natural sources from many decades. With a global urge to harness 'green energy' from renewable sources and recent development in low-powered wireless electronic devices which are portable, the field of EH has grabbed greater attention in the past few years. Batteries are widely used in many devices or systems; which makes us highly dependent on batteries as the primary power source. Emerging applications like wireless micro-sensor networks and micro electromechanical systems (MEMS) are couple of

technologies that could help in energy harvesting [1, 2]. There is the issue of the complexity and replacement of battery in many devices. A favourable solution to power-up these devices is to have a battery-less operation. But, in many cases, the life span of battery is limited to days or months, which is not economical. We can generate energy from the environment using energy harvesting for battery-less operations. Now, the challenge is to generate efficient and clean power for micro- to macro-level application. There are many ways by which energy can be harvested:

- Radiation (light, solar)
- Thermal (temperature gradient)
- Mechanical (potential, kinetic)
- Chemical (battery, fuel cell)
- Nuclear
- Magnetic
- Electric

Benefits of energy harvesting can be summarized as:

- Clean and renewable source of energy
- Long-term operability
- Cheaper
- Flexibility
- Maintenance free

1.3 An Energy System

An energy system consists of three stages: generation, conversion, and consumption. The energy generation stage requires an energy harvesting device along with an energy source, the storage technology that could be used to accumulate energy in excess from the harvester and provide it to the system in its place whenever energy is sufficient. The energy conversion stage requires power management circuitry and system that optimizes the harvested energy in the energy generation block to the energy consumption stage, the typical stages for energy harvesting are shown in Figure 1.

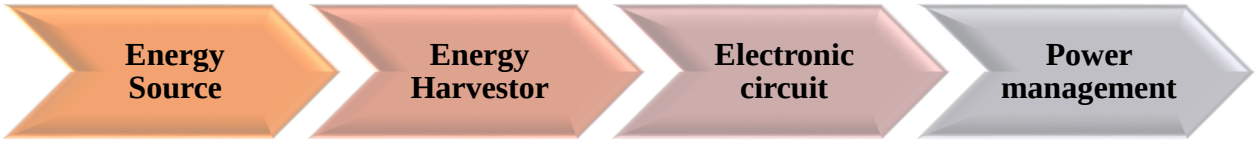

Figure 1.1 Block diagram for an energy harvesting system.

1.4 Vibrational Energy Harvesting

Mechanical energy sources can be found almost anywhere, and vibration sources such as ocean waves and human motion that converts mechanical energy into electrical energy is also an attractive approach. Many researches are developing a prototype for understanding power harvesting systems. Vibrational energy is available almost everywhere in the urban and industrial environment, but it is always overlooked as a source of power. The vibrational harvesters use one of three methods: electromagnetic, electrostatic or piezoelectric to harvest energy. The Table 1 gives an overview of the advantages and disadvantages of different transducers (electrostatic, electromagnetic, and piezoelectric) as reported in literature [3-5].

Table 1.1 Advantages and disadvantages of transducers

Transducers	**Advantage**	**Disadvantage**
Electrostatic	Smaller in size Mechanical resonance control	Requires separate voltage source Higher frequency than piezoelectric is needed Low output current
Electromagnetic	No voltage sources required Higher power output	Complex design Difficult to integrate into microsystems
Piezoelectric	Simple design No voltage source required Higher power output Small size High efficiency Precise mechanical control	Needs higher frequency Limited material selection Poor mechanical properties Low output current

Chapter - 2

Piezoelectricity

2.1 History of Piezoelectricity

Piezoelectricity is the mechanism of transfer of energy from mechanical (vibration) to electrical signal. The Charles Augustin de Coulomb in the late eighteenth century have been the first one who conjectured the idea that some solids might exhibit an electrical response when subjected to mechanical stress [6]. The Curie brothers; Pierre Curie and Jaques Curie have successfully demonstrated the piezoelectric effect in 1880. They provide the theory which correlates the mechanical stress in a crystal and the electrical effects resulting from change in temperature. To prove this, they have chosen some specific crystals like tourmaline, quartz, Rochelle salt for use in their experiment. They proved that when a crystal subjected to mechanical stress the surface charge gets appeared on the crystals; which is known as the piezoelectric 'direct' effect (piezo meaning "to press or squeeze"). They announced their finding as follows:

"Those crystals having one or more axes whose ends are unlike that is to say hemihedral crystals with oblique faces, have the special physical property of giving rise to two electrical poles of opposite signs at the extremities of these axes when they are subjected to a change in temperature: this is the phenomenon known under the name of pyroelectricity. We have found a new method for the development of polar electricity in these same crystals, consisting in subjecting them to variations in pressure along their hemihedral axes." [7]

The converse of piezoelectric effect that when an electric field is applied a stress is exhibited in a material has been verified by Gabriel Lippman in the year 1881.

The first practical application of piezoelectricity, has been development of sonar during World War I. To solve the problem of submarine detection the piezoelectric transducers has used by the French physicist Paul Langevin and his colleagues [6]. The 'crystal oscillator' has been the next major technological milestone in the advancement of piezoelectricity. Now a days piezoelectric based device are frequently used in our everyday electronic systems like radios, mobile, wristwatches, computers as well as oscillators and signal generators.

During World War II, many research groups in US, Russia and Japan developed man made piezoelectric material which have better piezoelectric properties than the naturally occurring

materials. Barium titanate ($BaTio_3$) is the first man-made piezoelectric substance that leads to the development of the lead zirconate titanate family of piezoceramics in the 1950s [8]. This results in the large number of applications and products like improved sonar devices, piezo buzzers, piezoelectric filters and microphones. The story does not end there, during the 1960s many discoveries have made on the piezoelectric properties and found that some polymers like Polyvinylidene also exhibit piezoelectric properties. This leads to the development of polymer based piezoelectric materials to this day. Apart from these applications mentioned above, the piezoelectric materials have been used in many technological applications like engine management system, medical ultrasonic devices and piezoelectric motors.

2.2 Piezoelectric effect

One can interpret piezoelectric effect only with an understanding of the internal structure of solids which exhibits it. A solid (sometimes called a crystalline solid) is characterised by long range order of the atoms, ions, or molecules that comprise it. The atoms, ions, or molecules are organized in a repeated pattern extending over all the three spatial dimensions, therefore the solid has a 'lattice' crystal structure. A 'unit cell' of the lattice structure can be defined as the smallest unit of arrangement of atoms. For example, Figure 2.1 below shows the unit cell of simple cubic lattice.

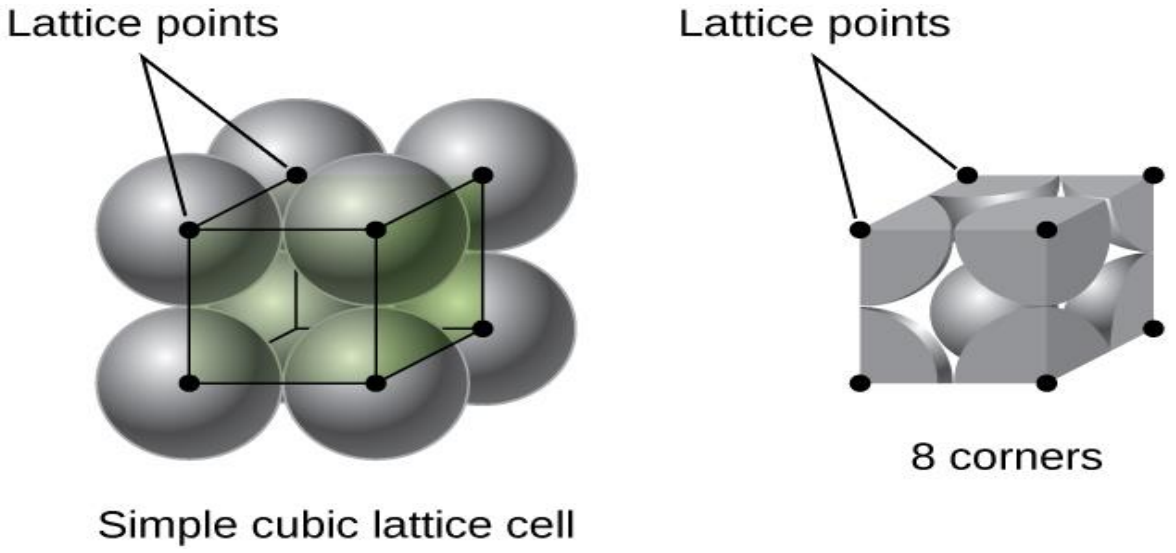

Figure 2.1 A unit cell of a simple cubic lattice [9]

Crystals are classified according to their symmetry; the cubic lattice is one of the seven lattice systems. Each system has a unique arrangement of three axes. The seven lattice systems are:

triclinic, monoclinic, orthorhombic, rhombohedral, tetragonal, hexagonal, and cubic. These systems can be further sub-divided into thirty-two 'point groups' according to their symmetry with respect to a point. Out of these thirty-two point groups, eleven are centrosymmetric and twenty-one are non-centrosymmetric. Out of these twenty-one; twenty non-centrosymmetric can fall into piezoelectric category. This non-Centro symmetry is a necessary condition for piezoelectricity. Due to this lack of symmetry, the crystal has the ability to form dipole when pressure is applied. Figure 2.2 below shows the characterisation of crystal system.

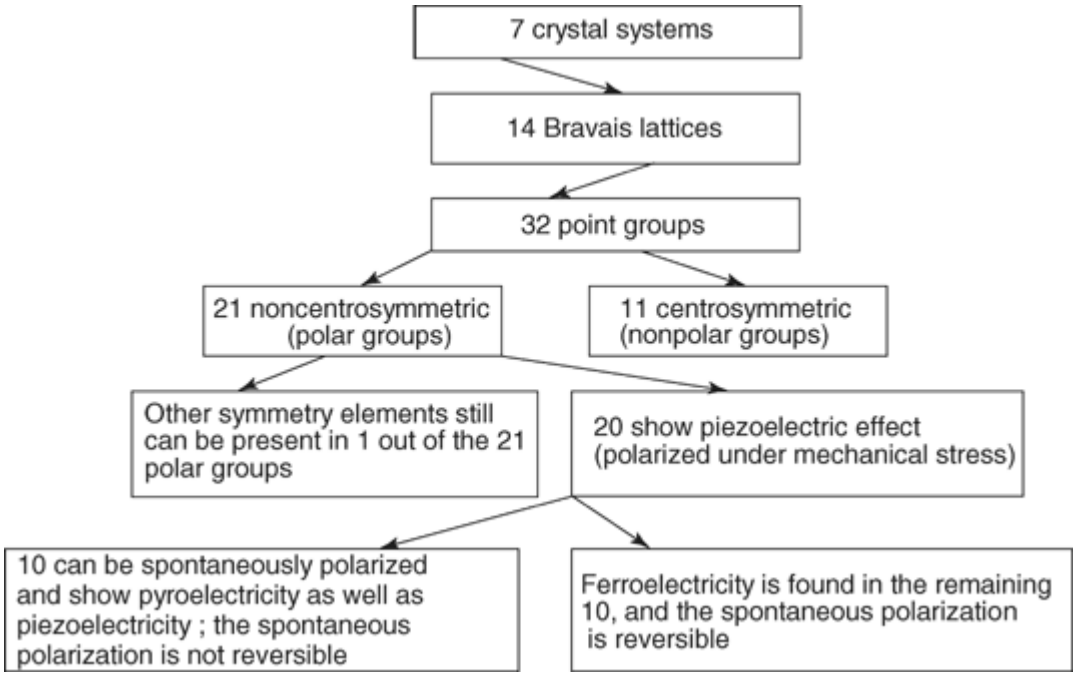

Figure 2.2 Categorisation of crystals belonging to the seven lattice systems [10].

As we know piezoelectric material is a combination of several unit cells and these unit cells have randomly oriented and distributed dipole moments. When a mechanical stress or an electric field is applied on a material, each dipole changes its orientation. The orientation of dipole moment is directly related to the piezoelectric effect. The alignment of dipoles is called poling which requires high electric field with thermal energy. When a high electric field is applied on a material, below a certain temperature called curie temperature, most dipoles aligned along the direction of the applied field. Figure 2.3 below shows a simple model explaining piezoelectric effect.

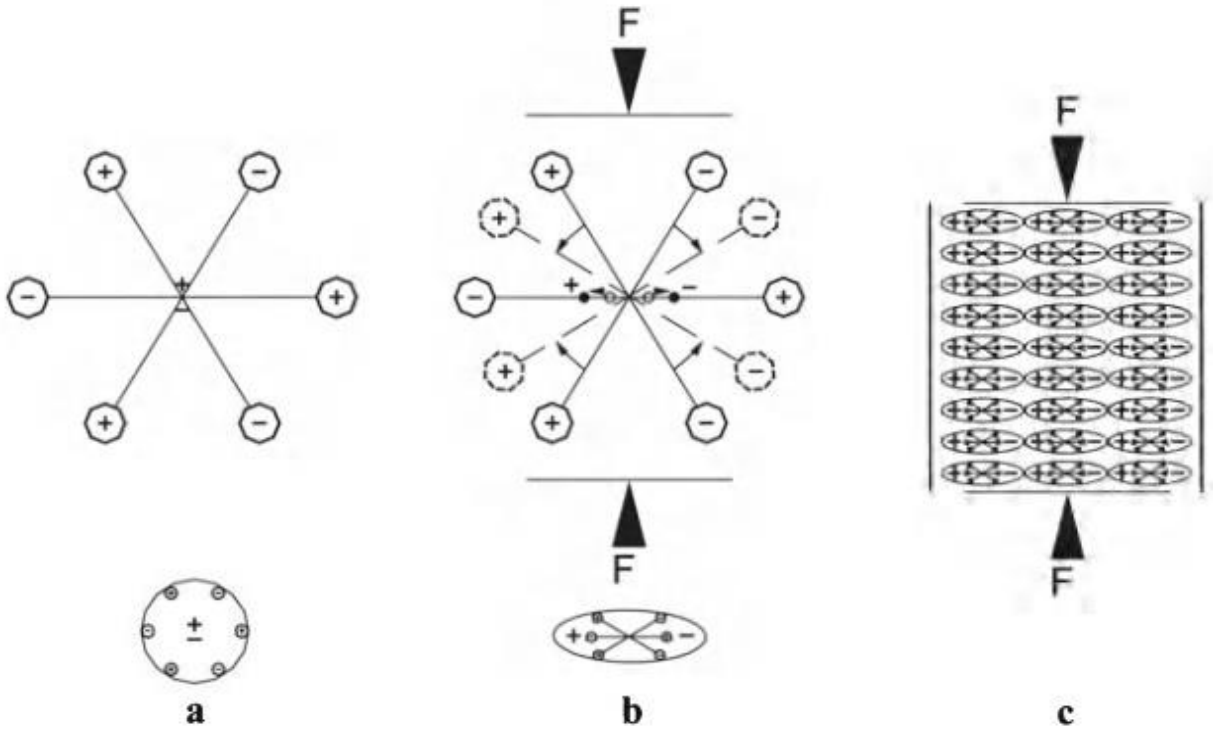

Figure 2.3 A simple molecular model explaining the piezoelectric effect: **a**) unperturbed molecule; **b)** molecule when subjected to an external force, and **c)** the polarizing effect on the surface of the material [11].

2.3 Lead-Free Piezoelectric Ceramics

Piezoelectric materials has numerous application in our daily life energy harvesting to medical imaging [12]. From the past sixty years, ferroelectric $Pb(Zr_{1-x}Ti_x)O_3$ ceramics is dominating the market for high performance actuators and transducers [12]. $Pb(Zr_{1-x}Ti_x)O_3$ ‘s reliable and outstanding properties are attributed to the temperature dependent morphotropic phase boundary(MPB), that separates the rhombohedral and tetragonal perovskite phases [12]. Lead zirconate titanate (PZT) shows excellent piezoelectric effect. But the European Union considering the toxicity of lead and lead based compounds passed a legislation for the development of environment friendly lead-free materials. The poisoning of lead has long been considered as threat to the health of a community because of its hazardous effects on mental and neurological development [13]. The main signs of lead poisoning include fatigue, muscle and joint aches, abdominal pain, etc. The scientists have been searching for lead-free piezoelectric materials from the past fifteen years and because of their intense effort the three

major ferroelectric solutions having comparable piezoelectric properties to those of PZT have been identified: the $(Bi_{1/2}Na_{1/2})TiO_3$-based [14, 15], the $(K_{0.5}Na_{0.5})NbO_3$-based [16, 17] and the $BaTiO_3$-based [18] compositions. Figure 2.4 schematically shows the d_{33} vs T_c of the three-lead free piezoelectric solid solutions.

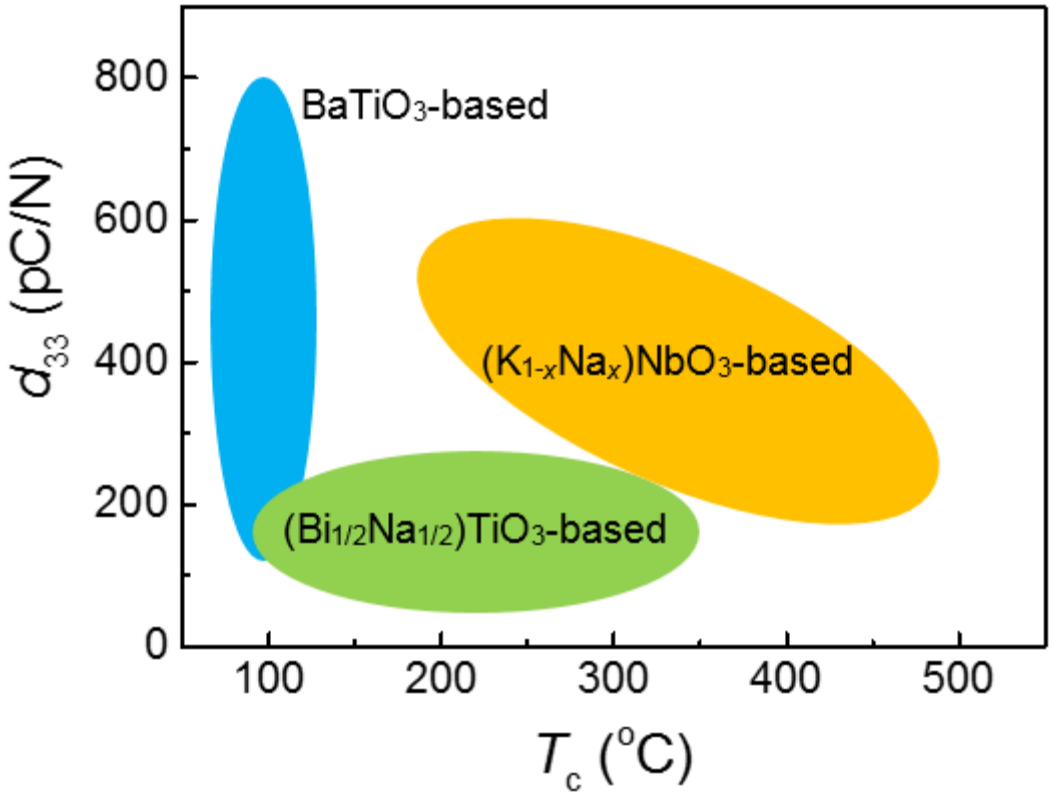

Figure 2.4 Schematic representation of d_{33} vs T_c of the three-lead free piezoelectric solid solutions [14].

The $BaTiO_3$-based ceramics shows outstanding piezoelectric properties (e.g. d_{33} > 600 pC/N) comparable to that of PZT.

2.4 $BaTiO_3$-based ceramics

The $BaTiO_3$ is the first simple oxide with ferroelectricity and because of its excellent dielectric properties it is dominating the ceramic capacitors in industry [19]. However, due to the phase boundaries at room temperature the pure $BaTiO_3$ does not show pleasing piezoelectric properties[20]. The exploration of $BaTiO_3$ based piezoelectric materials gets a kink in 2009 with the development of Ca- and Zr-doped compositions i.e., $Ba(Ti_{0.8}Zr_{0.2})O_3$–$(Ba_{0.7}Ca_{0.3})TiO_3$[18]. Because of the existence of a tricritical triple point the $Ba(Ti_{0.8}Zr_{0.2})O_3$–

$(Ba_{0.7}Ca_{0.3})TiO_3$ shows ultrahigh piezoelectric coefficients, d_{33} > 600 pC/N [18]. The $Ba(Ti_{0.8}Zr_{0.2})O_3$–$(Ba_{0.7}Ca_{0.3})TiO_3$ (BZT-BCT) solid solution have more complicated phase diagram (Figure 2.5) [21].

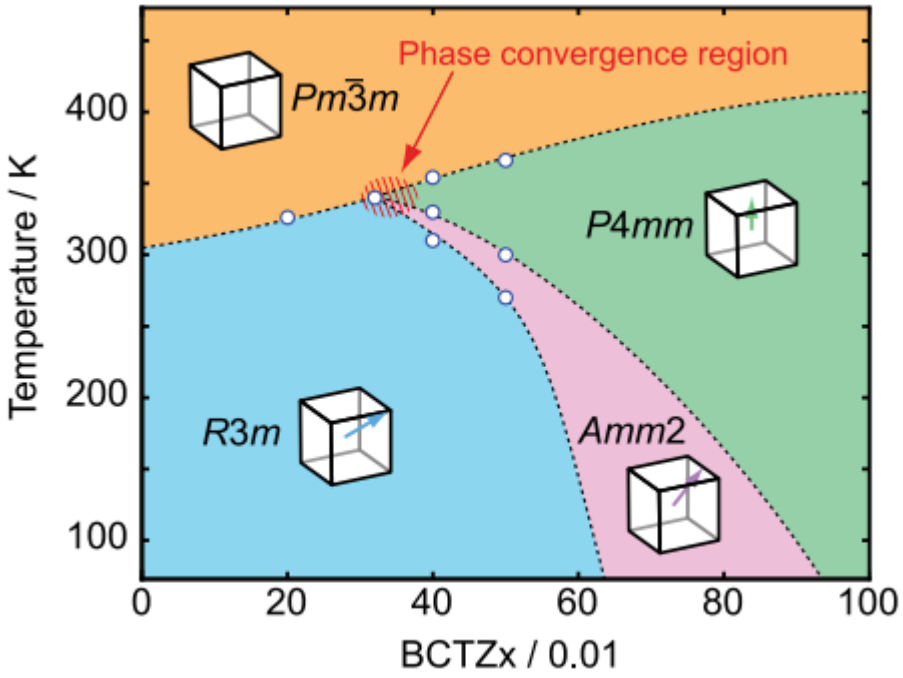

Figure 2.5 Phase diagram of BZT-BCT [21].

Based on this research, it is revealed that the high piezoelectric effect originates because of the orthorhombic phase [21].

2.4.1 Properties of BZT-BCT

- BZT-BCT have comparable electromechanical properties to that of PZT.
- It shows very high piezoelectric coefficient i.e., d_{33}~620 pC/N.
- It was reported that BCZT have very high dielectric constant value ~ 16480 at 10 kHz.

2.5 Polyvinylidene fluoride

Polyvinylidene fluoride (PVDF) shows piezoelectricity [22] and has 6.9 GPa of Young's modulus which is very low comparable to other piezoelectric material. PVDF is flexible than inorganic materials as it is a polymer and can have much higher energy density. PVDF exhibits piezoelectric coefficient(d_{33}) of -20 to 30 pC/N[23] and dielectric constant of 6-12 [24]. It is used in many biological systems and has very good biocompatibility. On the basis of chain confirmation structure, the polymer PVDF exists in α, β, γ and δ four crystalline phases. The

α-phase has zero net dipole moment because the dipoles are oriented anti-parallel to each other that is why it is non polar. The piezoelectricity arises in PVDF because of β and ɣ phase as β and ɣ phase is polar because dipoles are oriented parallel to each other making it polar.

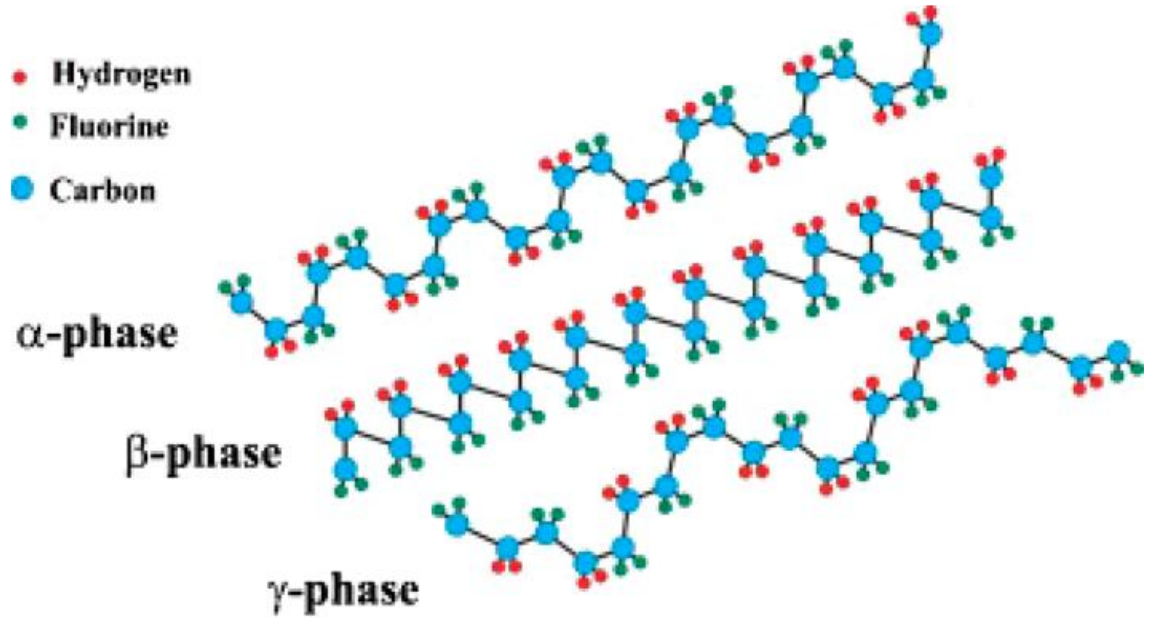

Figure 2.6 Representation different phase of PVDF [25].

Chapter – 3
Literature Review

This chapter includes the literature pertaining to the work of dissertation. We introduce different mechanical energy harvesting technologies and the focus is on piezoelectric energy harvesting. Some piezoelectric materials and their fundamental behaviours such as polarization orientation and piezoelectric coefficients are discussed earlier. The recent developments in the processing of piezoelectric energy and the methodologies to improve are checked. The questions which are in the literature are yet to be answered, are also identified.

The PZT (Lead zirconate titanate) for half a century; has become the technologically very important piezoelectric material [12]. PZT has very outstanding piezoelectric property yet because of Lead (Pb) toxicity it is currently facing global restrictions [26] . Hence, there is an urgent requirement of development of Lead free piezoelectric material that can challenge PZT, particularly with the most important high-end PZT with piezoelectric coefficient of d_{33}=500–600 pC/N) [27].

3.1 Literature Review on BCZT

Liu *et al.*, in 2009 have reported a lead free piezoelectric ceramic system $Ba(Ti_{0.8}Zr_{0.2})O_3$-$(Ba_{0.7}Ca_{0.3})TiO_3$ which exhibits a very high piezoelectric coefficient of d_{33}=620 pC/N [18]. They designed a system of BZT-xBCT, where x is molar proportion of BCT. Samples are fabricated by a traditional solid-state reaction method. The calcination is performed at 1350℃ and sintering at 1450℃-1500℃ in air. It is observed that the morphotropic phase boundary (MPB) as shown in the phase diagram (Figure 3.1). The 50BCT has critical temperature (T_C)~93℃, very soft in nature, have a very high permittivity ε~ 3060, very low coercive field Ec of 168 V/mm that is why it shows significantly very high d_{33} of 520-620 pC/N.

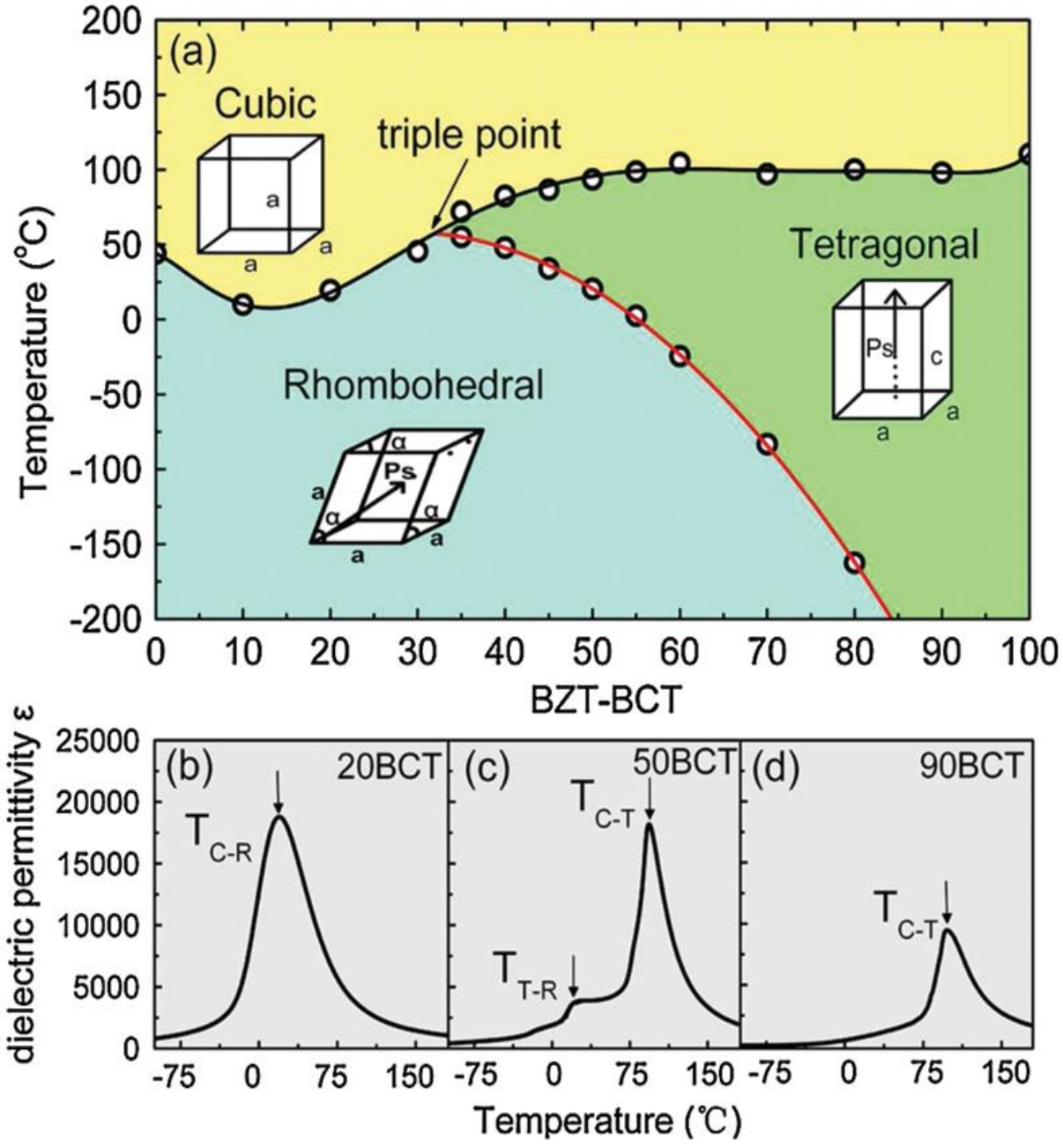

Figure 3.1 (a) Phase diagram of piezoelectric $Ba(Ti_{0.8}Zr_{0.2})O_3$-$(Ba_{0.7}Ca_{0.3})TiO_3$ **(b)–(d)** Dielectric permittivity curves for 20BCT, 50BCT, and 90BCT, respectively [18].

Bao *et al.*, 2010 [28] have reported a method of increasing the T_C of lead free BZT–*x*BCT which is increasing the T_C of both tetragonal and rhombohedral terminals. They have used $Ba(Zr_{0.15}Ti_{0.85})O_3$–$x(Ba_{0.8}Ca_{0.2})TiO_3$ composition and shows a higher T_C of 114℃ at x= 53. They also found that with a deviation from the cubic–tetragonal–rhombohedral triple point the both d_{33} and ε along the MPB decreases. There is improvement by using $BZ_{15}T$–$53BC_{20}T$ composition and exhibits a high T_C of 114 ℃ that is 21℃ higher than that reported for BZT–

50BCT as shown in the figure 3.2 of temperature dependence of composition, but it has a lower piezoelectric coefficient d_{33}=450 pC/N and dielectric permittivity ε~ 2252.

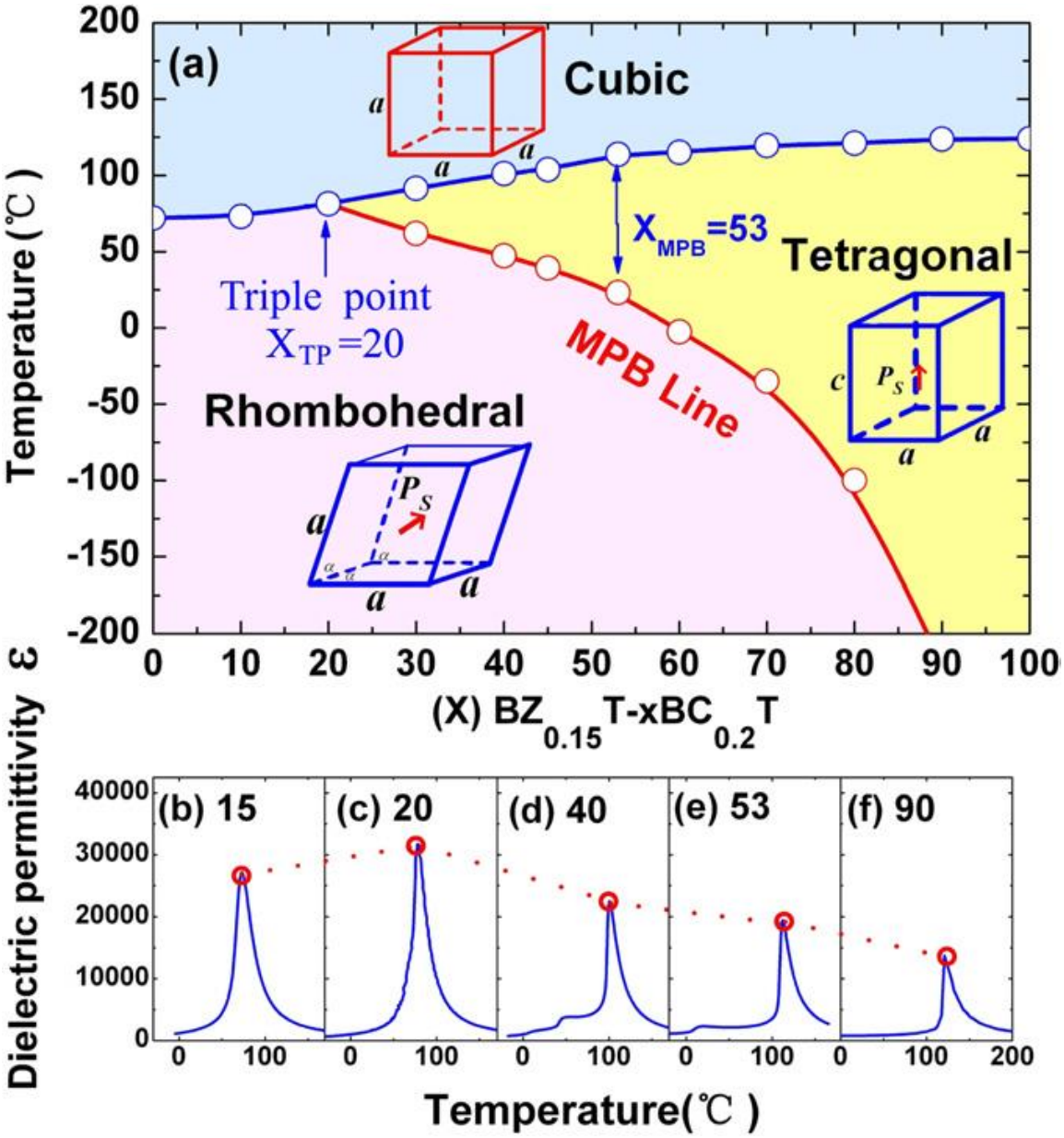

Figure 3.2 (a) Temperature–composition phase diagram of the ceramics $BZ_{15}T$–$xBC_{20}T$, showing the cubic paraelectric phase, ferroelectric rhombohedral and tetragonal phase. **(*b*)–(*f*)** The temperature dependence of dielectric permittivity for $BZ_{15}T$–$xBC_{20}T$ (x = 15, 20, 40, 53, 90) [28].

Xue *et al.*, in 2011 [29] have measured piezoelectric, elastic and dielectric properties for the MPB composition, $Ba(Zr_{0.2}Ti_{0.8})O_3$-$50(Ba_{0.7}Ca_{0.3})TiO_3$ (BZT-50BCT). For a fixed composition any change in temperature will cause the system to go away from the MPB and degrades the piezoelectric property. The ceramic samples BZT-50BCT used at the MPB regime

at room temperature. Figure 3.3 below shows the temperature dependence of piezoelectric constant (d_{33}) and the electrochemical coupling factor (k_{33}). They conclude that the piezoelectric properties are optimal only around room temperature and they decrease when deviated from MPB regime (around room temperature). On lowering the temperature from room temperature to -50°C, the d_{33} value drops from 546 to 93 pC/N, and the k_{33} value gets decreases from 65 to 38%. The point of interest is that BZT-50BCT can exhibit appreciable piezoelectric properties even at low temperature (-50°C). At such a low temperature, the spontaneous polarization P_m is 17.9 μC/cm^2 [figure 3.3(b)], the remnant polarization P_r is 12.9 μC/cm^2 [Figure 3.3(c)], the coercive field E_c is 354 V/mm [Figure 3.3(d)], and the d_{33} is 93 pC/N.

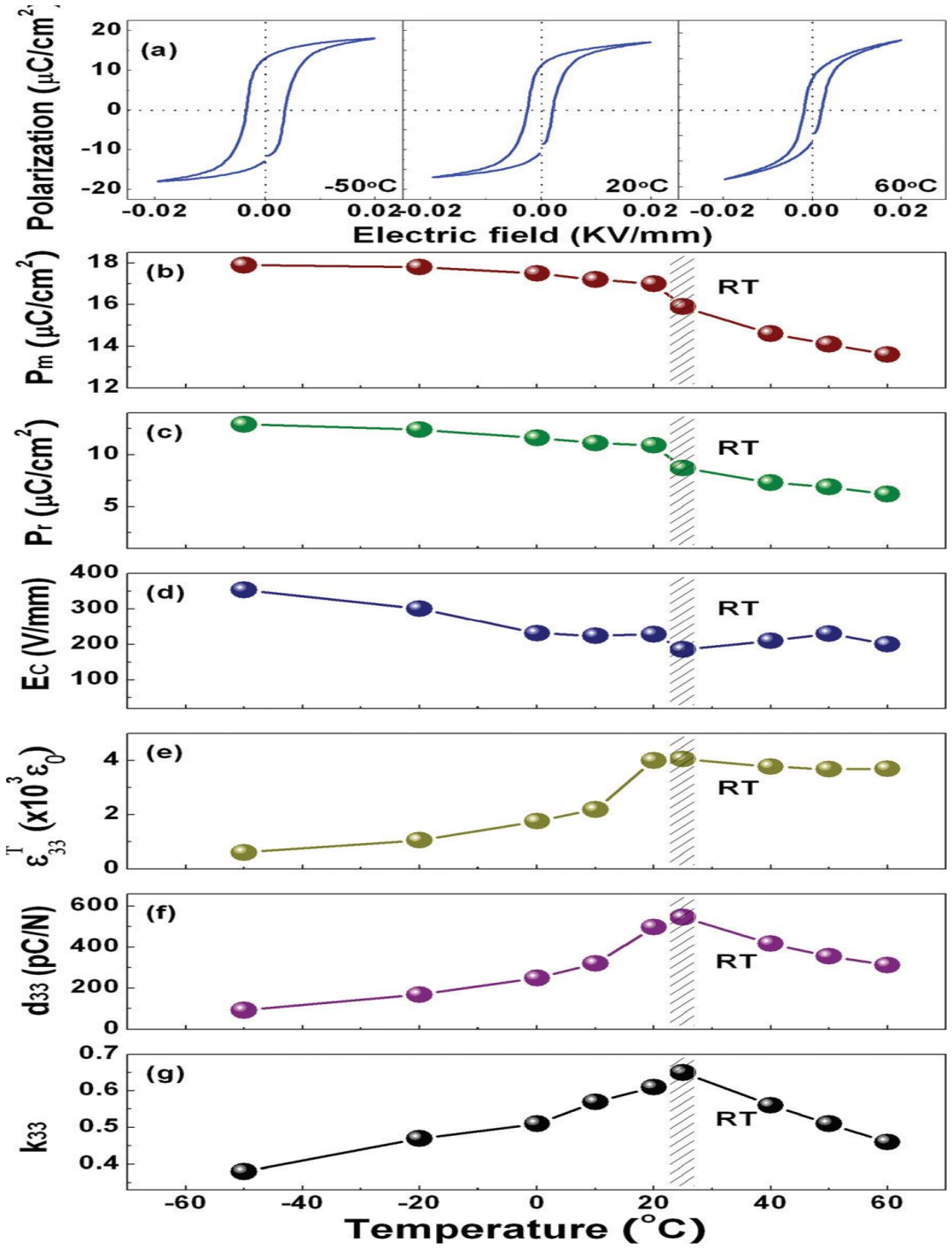

Figure 3.3 (a) Hysteresis loops of BZT-50BCT at a temperature of 60, 20, and-50°C, respectively. The temperature dependence of **(b)** saturation polarization P_m, **(c)** remnant polarization P_r, **(d)** coercive field E_c, **(e)** permittivity ε^T_{33}, **(f)** piezoelectric coefficients d_{33}, and **(g)** electromechanically couple factor k_{33} [29], for the 50BCT-BZT sample.

Praveen *et al.*, in 2015 [30] have investigated the effect of poling process on piezoelectric ceramics [*x*BZT–(1−*x*)BCT] ($0.48 \leq x \leq 0.52$) synthesized by sol–gel method. Crystalline

powders with single-phase perovskite structure has been calcinated at 700℃ and sintered at 1450℃. Electrical poling is a process in which reorientation of domain and movement of domain wall takes place which when performed for ferroelectric ceramics leads in improvement of their piezoelectric properties [31]. So, for enhanced piezoelectric response it is necessary to optimize the poling conditions like temperature, electric field and poling time. The authors concluded that on optimising the poling condition the composition of 0.5BZT–0.5BCT, at the Morphotropic phase boundary shows very high coercive field (E_c) of 0.14 kV/mm and remnant polarization (P_r) of 12.2 μC/cm^2, d_{33} nearly 637 PC/N and has large coupling coefficient kp nearly 59.6%, a high piezoelectric voltage constant g_{33}~29 mV m/N.

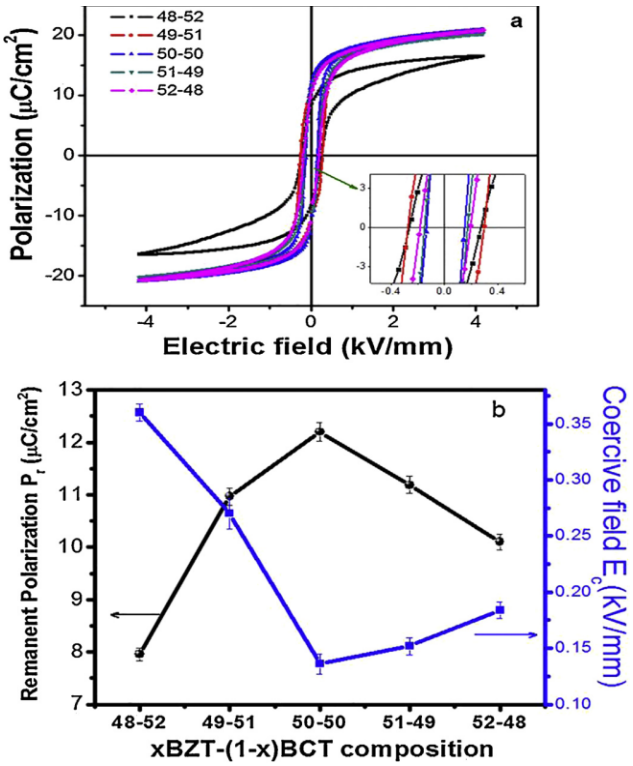

Figure 3.4 (a) Polarization and current vs electric field –hysteresis loop of [*x*BZT–(1−*x*)BCT] where, *x* = 0.48–0.52 sintered (1450℃) and **(b)** Variation of remnant polarization and coercive field as a function of composition sintered at 1450℃ [30].

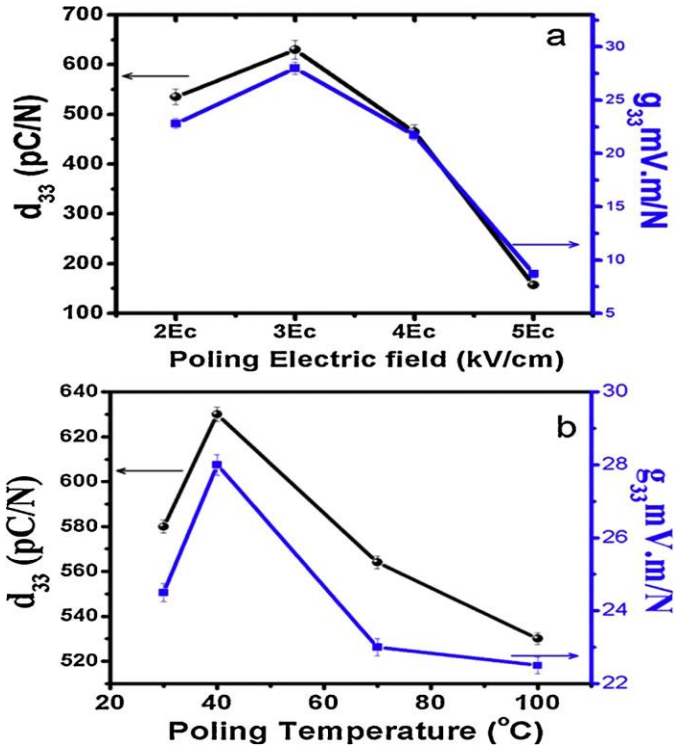

Figure 3.5 (a) Variation of piezoelectric charge coefficient and piezoelectric voltage coefficient as a function of poling field of 0.5BZT–0.5BCT sintered (1450℃), poled at *T*p~ 40℃. **(b)** Variation of piezoelectric with poling temperature [30].

Bai et al., in 2015 [32] have reported that Lead-free piezoelectric compositions based on (Ba,Ca)(Zr,Ti)O_3 exhibit many piezoelectric properties which are similar to the conventionally used Pb(Zr,Ti)O_3 materials. They investigated a wide range of processing factors such as composition (e.g. ratio of Ba(Zr,Ti)O_3 to (Ba,Ca)TiO_3), sintering conditions (temperature and cooling rate), particle size of the calcined ceramic powder, structure and microstructure (e.g. phase, lattice parameters, density and grain size), and their effect on the piezoelectric properties of BCZT. A wide range of BZT/BCT composite ceramic have been fabricated at various sintering temperatures with variety of procedures. Highly densed ceramics samples are produced and the average size of the sintered grain has been controlled by adjusting the initial particle size of the powder, sintering temperature and the rate of cooling during sintering. It is shown that the c/a ratio particularly of the tetragonal phase is independent of sintering temperature. The tentative phase diagram based on phase transitions and the dielectric measurement is constructed, which is consistent with previous reports shown in Figure 3.7. The piezoelectric properties can be modified by variations of c/a tetragonal phase ratio and grain size for particular compositions. Values of d_{33} can be seen to increase with c/a ratio,

whereas it has been suggested that there is grain size limit or threshold above which the platue of d_{33} values even begin to decline.

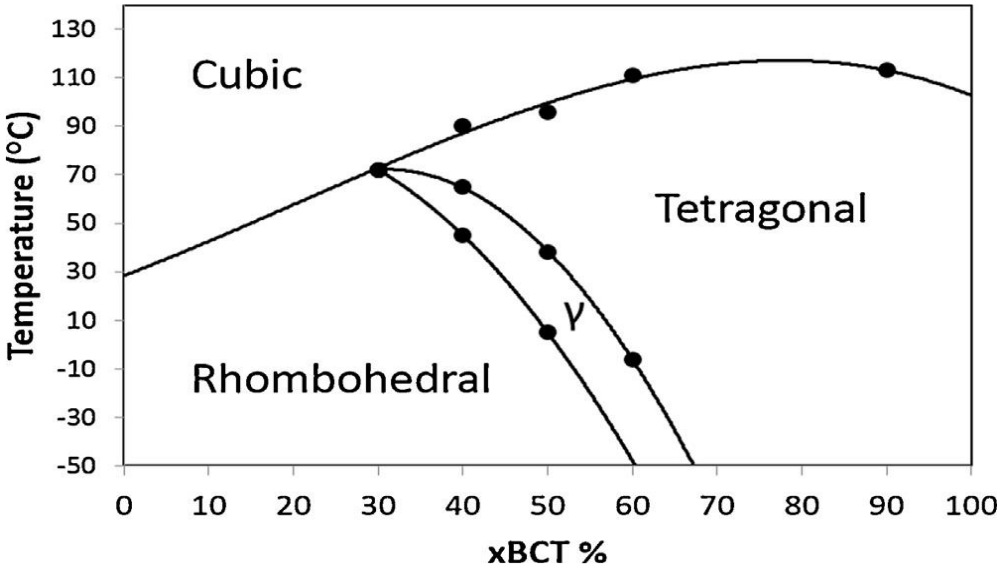

Figure 3.6 Tentative Phase diagram of the BZT–BCT solid-solution [32].

Castkova *et al.,* in 2015 [33] reported an investigation of piezoelectric properties of $Ba_{0.85}Ca_{0.15}Zr_{0.1}Ti_{0.9}O_3$ (BCZT) powders prepared by three wet chemical synthesis routes, co-precipitation, glycine and sol–gel. The sol-gel method is very successful method for the preparation of BCZT nanoparticles having tetragonal perovskite phase. They concluded that the grain size can reduced to 0.8μm. The samples having grain size ≤1.4 μm possess extremely small or zero d_{33} value. The ceramics prepared from sol–gel powder sintered at 1425°C having theoretical density of 89.6% and grain size of 36 μm shows highest d_{33}=410.8 ±13.2 pC/N.

Wang *et al.,* 2016 [34] have studied Lead free $(Ba_{0.85}Ca_{0.15})(Ti_{0.9}Zr_{0.1})O_3$ (BCZT) ceramics prepared by the sol–gel method (SG) and solid-state method (SS). It is found that the concentration of Ti, acetic acid and bathing temperature of sol have the impact of different level for ferroelectric and dielectric properties of BCZT ceramics. The calcination was done at 1000°C and sintered at 1420°C to produce very dense BCZT ceramic having fine grain size. The optimum electrical performances showed by BCZT-SG have the value of d_{33} = 504 pC/N, K_p = 0.56, ε_m=16,480, P_s = 17.76 μC/cm^2, Pr = 11.64 μC/cm^2, the energy density (W)= 0.52 J/cm^3.

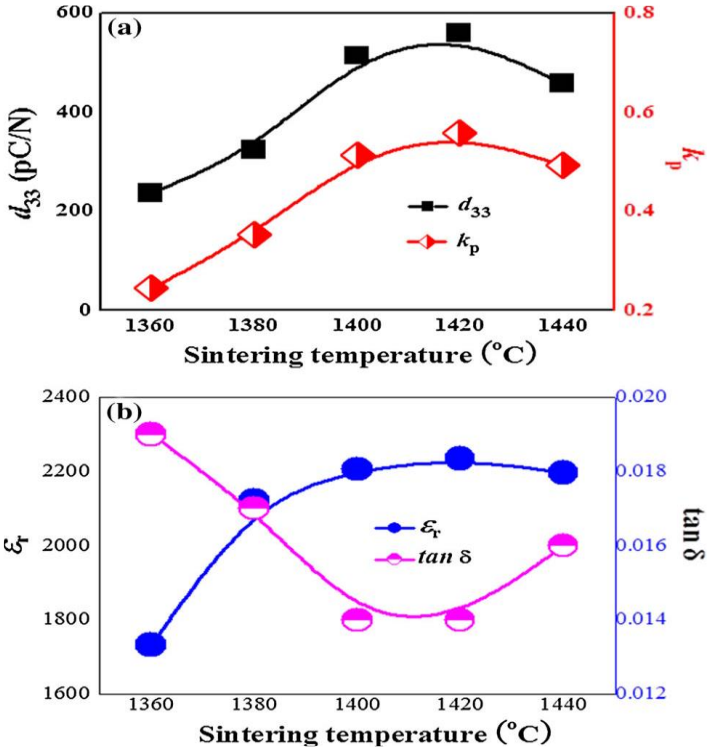

Figure 3.7 (**a)** d_{33} and k_p, (**b)** ε_r and tan δ of BCZT ceramics prepared by sol–gel method calcined at 1000 ℃ with various sintering temperatures [34].

Zhang *et al.*, 2019 [35] have investigated the effect of porosity on the microstructure, piezoelectric, and dielectric properties of the porous lead free barium calcium zirconate titanate $0.5Ba(Ca_{0.8}Zr_{0.2})O_3$-$0.5(Ba_{0.7}Ca_{0.3})TiO_3$ (BCZT) ferroelectric ceramics. They fabricated the ceramic via a burnt polymer spheres (BURPS) technique by introducing corn starch as the pore-forming agent. The ceramics are prepared by a solid-state reaction approach and the BURPS technique (Burnt Polymer Spheres). Afterwards the mixtures were calcined at 1200 °C for 3h and 4h of ball-milling, followed by additional ball-milling of 24h.They mixed the milled powder with ethanol for 12h and add the corn starch powder with different wt%. The sintering is performed at 1400°C for 4h. It is found that the relative permittivity of the porous BCZT dropped from 2158 to 1026, while dense ceramics have shown a relative permittivity of 2590. As the porosity increases from 10% to 25% the hydrostatic charge coefficient(d_h) increases from 140 to 560% which is higher than the dense BCZT material. They demonstrated lead free porous $0.5Ba(Ca_{0.8}Zr_{0.2})O_30.5(Ba_{0.7}Ca_{0.3})TiO_3$ ceramics shows d_h~93 pC/N, g_h~ 10.237×1012 Vm/N and $d_h \cdot g_h$~0.952×1012 m^2/N at the maximum level of 25% porosity.

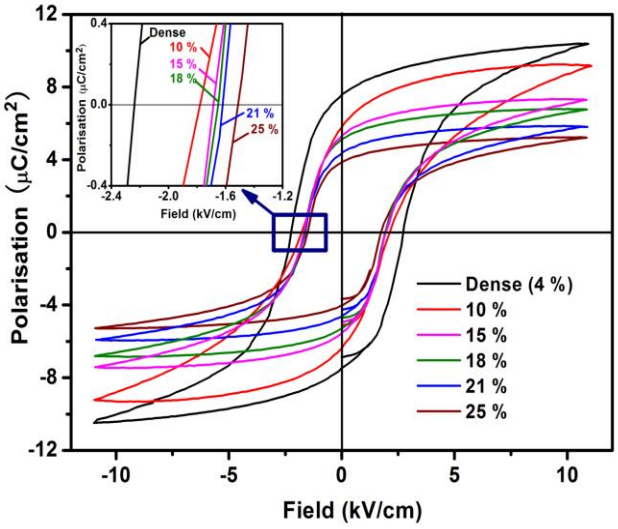

Figure 3.8 Ferroelectric hysteresis loop of dense and porous BCZT with different porosities [35].

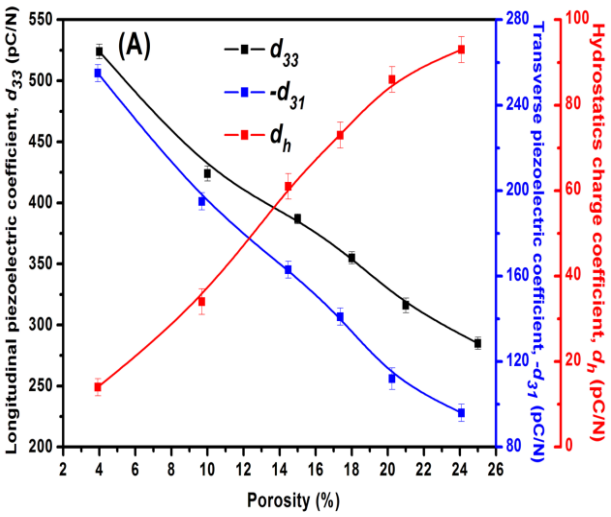

Figure 3.9 Piezoelectric coefficients of porous BCZT with porosity ranging from 10-25% [35].

Parjansari *et al.*, 2019 [36] have investigated the improvement in electrical properties of $Ba_{0.85}Ca_{0.15}Zr_{0.10}Ti_{0.90}O_3$ (BCZT)-x seed ceramics, where BCZT seed (x) = 0.0, 1.0, 2.0, 3.0 and 4.0 molar percentage. The seed-induced method is the new methodology for the stabilisation of perovskite phase and in this method the fabrication can be done at lower temperature. On addition of seed compound the perovskite phase gets formed at low temperature with the decrease in energy barrier of phase formation[37]. The calcination was performed at 1200°C for 2h and sintering at 1450°C for 4h. The sample with seed content of 3.0 molar percentage had the highest values of density, d_{33} and thickness electromechanical coupling coefficient (k_t) at 5.7 g/cm3, 520 pC/N and 48%, respectively.

From the literature review it can be inferred that availability of literature on BCZT is scarce. Hence, there is lot of scope of further studies in terms of achieving better and useful results as it is proven that BCZT is one of the best lead-free piezoelectric material.

3.2 Literature on PVDF

Martins *et al.,* 2014 [38] have investigated the electroactive properties of poly(vinylidene fluoride), PVDF, and its wide range of application in biomedicine, energy generation and storage and many others. PVDF, and its copolymers are the family of polymers which has the highest dielectric constant and electroactive response, including piezoelectric, pyroelectric and ferroelectric effects. They concluded that the polymer should be in of its electroactive phase for many applications. They have suggested the main characteristics of the electroactive phases of PVDF and its copolymers, the experimental technique for their identification in proper way along with the processing strategies to achieve the desired characteristics of the materials. PVDF and its composites shows outstanding electrical properties among polymers which can certainly support the most challenging application of the near future.

Mahale *et al.*, 2018 [39] have studied the development of β-phase in spin-coated PVDF thick films. They conducted a study of the effect of variation in baking temperature and in spin speed on β-phase content in the spin-coated PVDF thick films (∼4−25μm). The β-phase development dependents on crystallization temperature and film stretching. The crystallisation temperature was adjusted by means of baking and stretching is achieved by spinning. Up to the baking temperature of 60°C the β-phase is dominant. After 60°C the β-phase starts decreasing and α-phase starts increasing. The α-phase is dominant at 90°C. With the increase in baking temperature the porosity decreases.

Patra *et al.,* 2018 [40] have analysed the structural, dielectric and ferroelectric properties of the Polyvinylpyrrolidone modified Barium Zirconate Titanate /PVDF nanocomposites as Self-Powered Sensor. The simple tape casting technique is used to fabricate the Polyvinylpyrrolidone (PVP) modified BCT-BZT/PVDF nanocomposites followed by hot press technique. The crystalline BCT-BZT powders are prepared by a simple sol-gel method. Addition of PVP modified BCT-BZT powders improves the polar phase in PVDF matrix. The Rietveld refinement analysis confirmed the coexistence of orthorhombic and tetragonal phase in the synthesized powders. They investigated the piezoelectric output response as a function of different weight percentage of ceramic powders in the PVDF matrix and found that the device with 60 wt% PVP modified BCT-BZT powders exhibited maximum peak to peak voltage of 23 V when tested for harnessing waste biomechanical energy. The device is flexible,

light-weight and environment friendly. And it can be investigated as the possible applicant for application as self-powered sensor.

Table 3.1 Summary of some important parameters

Reference	year	D_{33}(pC/N)	ε	P_r(μC/cm^2)	Ec (V/mm)	Energy storage density(J/cm^3)	Calcination temperature (℃)	Sintering temperature (℃)
[18]	2009	620	3060	…	168	…	1350	1450-1500
[28]	2010	450	2252	…	…	…	1300	1450
[29]	2011	93	…	12.9	354	…	1350	1450
[30]	2015	637	…	12.2	140	…	700	1450
[33]	2015	410.8 ±13.2	…	…	…	…	…	1425
[34]	2016	504	16480	11.64	…	0.52	1000	1420
[35]	2019	93	1026	…	…	…	1200	1400
[36]	2019	520	…	…	…	…	1200	1450

Chapter – 4

Experimental details

4.1 Synthesis of BCZT nanoceramics

The sol-gel method was used to synthesize $Ba_{0.85}Ca_{0.15}Ti_{0.9}Zr_{0.1}O_3$ (BCZT). The starting materials were Zirconium oxychloride ($ZrOCl_2$.$8H_2O$), Barium acetate (Ba ($CH_3COO)_2$), titanium isopropoxide ($C_{12}H_{28}O_4Ti$) and calcium nitrate tetra hydrate ($Ca(NO_3)_2.4H_2O$) used for the synthesis of BCZT nanoceramics. Stoichiometric ratio of Zirconium oxychloride ($ZrOCl_2$.$8H_2O$) and the calcium nitrate tetra hydrate (Ca ($NO_3)_2.4H_2O$) were dissolved in ethanol separately; the mixture is then stirred for 30 minutes until the solution become transparent. Then stoichiometric compositions of Barium acetate ($Ba(CH_3COO)_2$) was mixed in the acetic acid and kept stirring for 30 minutes until it dissolved completely. Add the required amount of titanium isopropoxide ($C_{12}H_{28}O_4Ti$) in the solution; after addition white solution was formed which then stirred continuously overnight at 80°C; to obtain white gel is. Further, the gel was dried at 100°C and the solidified lumps were grounded into the fine powder by using agate mortar and pestle. Figure 4.1 shows the flow chart of preparation of BCZT.

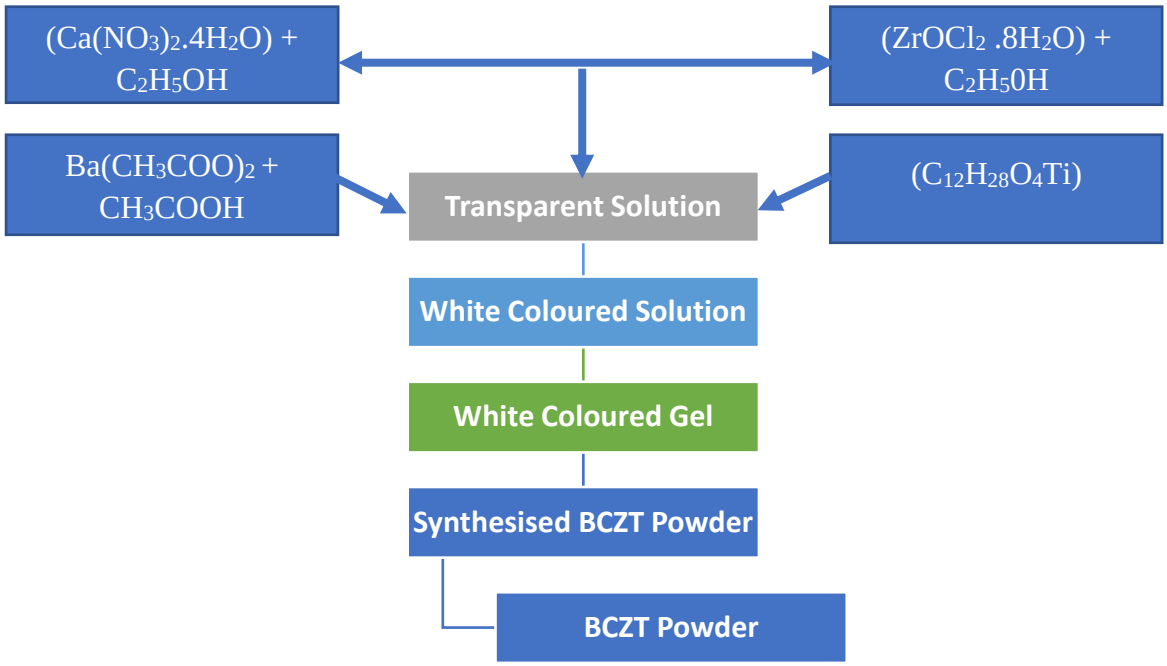

Figure 4.1 Flow chart of synthesis of BCZT nanoceramics.

The synthesized powder was calcined at 900°C for 3 hours in order to remove unreacted materials and impurities. The synthesized BCZT powder is shown in Figure 4.2 in pellet form. The calcined powder was scanned with x-ray diffraction to confirm the phase formation.

Figure 4.2 BCZT powder in pellet form.

4.2 Syntheses of PVDF thin films

4.2.1 Materials

ALDRICH with average Mw 534,000 was used to prepare PVDF which is further used for the preparation of thin films using N, N-dimethyl formamide (DMF) (LOBA CHEMIE) as a solvent.

4.2.2 Synthesis of homogenous solution of PVDF

Dimethyl formamide (DMF) is one of the best solvents in which PVDF gets disappeared after dissolving. This solvent helps in preparing thin films having less porosity and higher evaporation rate. The PVDF concentration depends on the viscosity we need, in a 6 ml of DMF 40% of PVDF is added to make homogeneous solution. The solution was placed on hotplate and stirred continuously for 1 h for the complete dissolution of PVDF.

4.2.3 Synthesis of the PVDF films by tape casting method

The prepared solution was poured on the glass plate. Then the films of PVDF of different thickness were fabricated using doctor blade. The formed films were dried at 90℃. When the films get completely dried it is removed from the glass plate. This leads to the formation of transparent and thick films of PVDF.

Figure 4.3 PVDF thin film.

4.3 Fabrication of BCZT/PVDF composite films

The sol gel method as used to synthesize BCZT/PVDF composite films. The obtained PVDF powder was converted into a sol form. A solvent DMF was used to dissolve PVDF polymer and kept at 90℃. Further in the DMF; BCZT powder were added and then sonicated for 1 h so that the powder gets completely dissolved into PVDF. Again, the solution was kept on hot plate and stirred until the solvent gets evaporated lead to the formation of gel. A composite film of BCZT/PVDF was prepared by pouring gel on glass plate and fabricated using doctor blade. To get the desired film having no porosity a wide range of concentration of 20%, 30%, 40%, and 50% by weight of BCZT was prepared. Figure 4.4 shows composite films of PVDF/BCZT.

Figure 4.4 Composite films of PVDF/BCZT.

4.4 characteristics

The phase composition of the given sample has been determined by using X-ray diffractometer ("PNAlytical X'Pert-Pro MPD PW3040/60) having range 3^0 to 100^0 and step size 0.02. Further Scanning electron microscope (SEM, JEOL) is used to study surface morphology.

4.4.1 X-ray Diffractometry (XRD)

For the determination of grain size, solution composition, degree of the crystallinity and network constants in crystalline substance X−ray Powder Diffraction (XRD) is a used. It helps in studying the atomic spacing, crystal structure, crystal dimensions, phase analysis and lattice parameters. To know the structure and properties of synthesized material this data is very useful.

The diffraction totally depends on the constructive interference between the crystalline samples and the monochromatic X-rays. Cathode ray tube produces the X-rays, the electron having sufficient energy ejects the electrons from the inner shell of the target material that produces characteristic x-ray spectra. The K_α and K_β are the most common characteristic X-ray spectra. The monochromatic radiation is produces by these X-rays. Copper is one of the most common material used as target material, having Cu K_α radiation's wavelength equals to 1.5418Å. Collimated X-rays are made to concentrate and directed towards the given sample. There is the constructive interference between the X-rays and the sample satisfying the conditions of Bragg's law ($n\lambda = 2d\sin\theta$) shown in Figure 4.5 (a). The rays after diffraction are detected, processed and then counted. The diffraction patterns are obtained with a range of 2θ angles after the scanning of sample. The mineral is identified with the help of d-spacing [41].

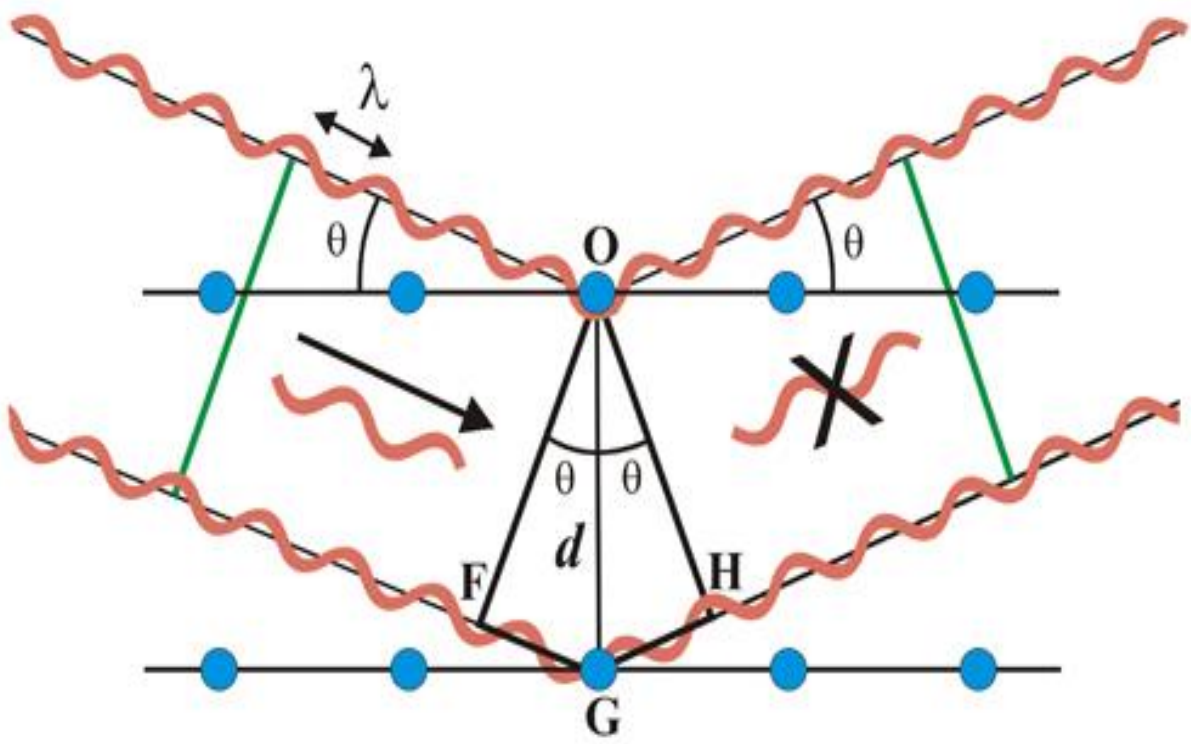

Figure 4.5 (a) Schematic of Bragg's law from a crystal [42].

Figure 4.5 (b) Experimental set-up of XRD [43].

Specification

Model	: "PANalytical X'Pert-Pro MPD PW3040/60 XRD"
X−Ray Power	: 2 kW
Source	: Cu target X−Ray tube
2θ° Measurement range	: 30 to 100
Accuracy	: ± 0.0025

4.4.4 Scanning electron microscope (SEM)

For the study of microstructure of the sample the scanning electron microscope is used. Electron column, scanning systems, detectors, vacuum system and electronic controls are the main parts of SEM. The high energy electron beam is produced by the electron gun which is then focussed by electron lenses onto the specimen. An electromagnetic radiation is emitted when an accelerated electron hits the specimen surface which is used to analyse structural constituents and the image formation. The detector detects three types of electrons, firstly from the back scattered electrons having changed direction, secondly those electron which does not undergo change in kinetic energy, lastly from those which undergo inelastic scattering due to which they impart some of their kinetic energy to the target electron that results in decrease in kinetic energy. The detector collects the signals which is then amplified and displayed on the monitor [44]. Figure 4.6 shows the experimental set up of SEM.

Figure 4.6 Experimental setup of SEM [45].

Specifications

Model	: JEOL SEM
Accelerating voltage	: 0.5 kV to 30 kV
Magnification	: × 5 to × 300,000
Resolution	: 3.0 nm（30 kV）、8 nm（3 kV）、15 nm（1 kV）

Chapter - 5

Results and discussions

5.1 X-ray diffraction (XRD) analysis

Figure 5.1 shows the X-ray diffraction pattern of the xBZT-(1-x)BCT ceramics where x= 0.5 calcined at 1000℃ for 3h. The strong XRD peaks having a small full width at half maxima (FWHM) i.e., **β**, this indicates that the synthesized powders are well crystallized. The diffraction pattern of $BaTiO_3$ based BCZT ceramic shows good agreement with the perovskite structure of $BaTiO_3$ with the P4mm space group and the obtained pattern is indexed using ICDS NO.-01-089-1428 of cubical structure. The peaks are observed at 2θ = 22.17º, 31.54º, 38.88º, 45.20º, 50.88º, 56.11º, 65.77º respectively. The corresponding planes or Miller index (hkl) to the observed peak are (100), (110), (111), (200), (210), (211), (220) respectively[30].

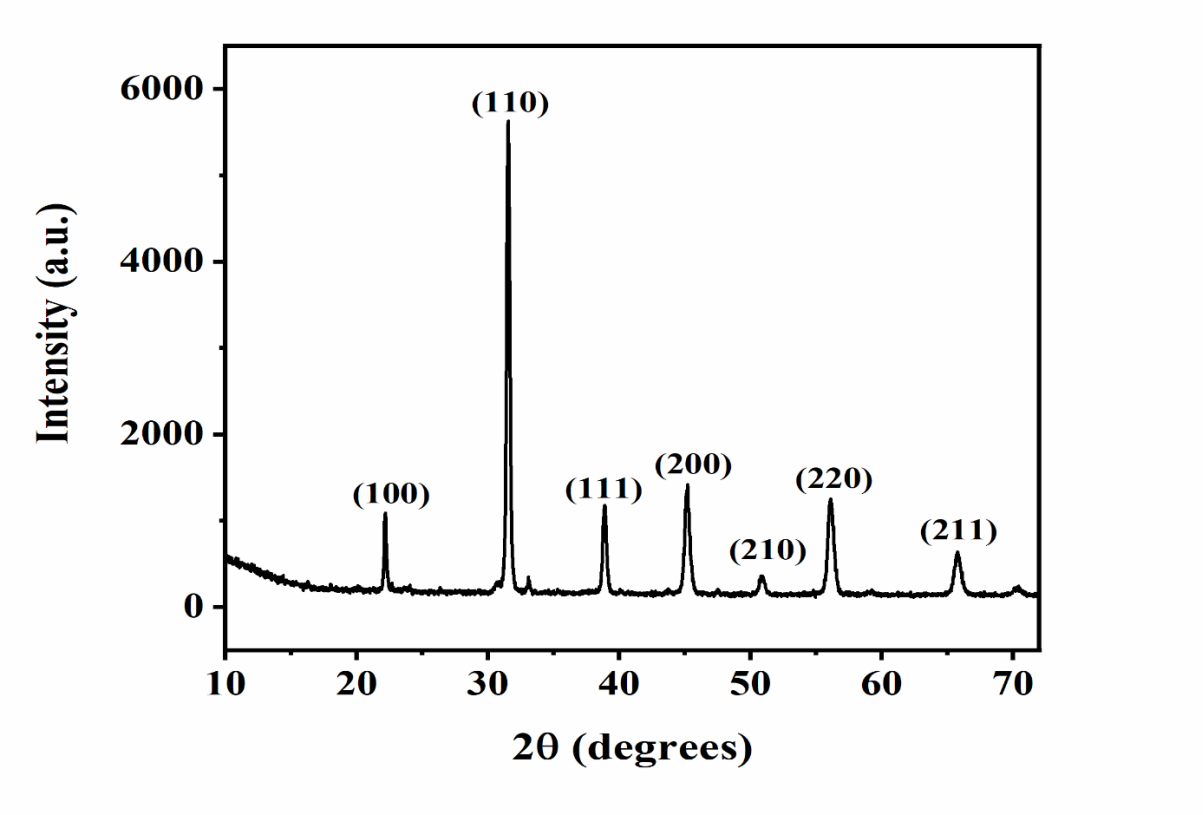

Figure 5.1 X-ray diffraction pattern of BCZT ceramics calcined at 1000℃ for 3 h.

The Debye-Scherrer formula (Equation 5.1) is used to find the crystallite size (t) of the calcined powder.

$$t = 0.9\lambda / \beta\cos\theta \qquad \textbf{(5.1)}$$

where, λ is the wavelength of used x-rays, 0.9 is shape factor, θ is the Bragg's angle and β is full width at half maxima (FWHM). The crystallite size obtained for corresponding 2θ values are shown in table 5.1. The average crystallite size obtained is~ 26nm.

Table 5.1 Crystallite size at different θ values

Θ(radian)	(hkl)	B(radian)	t(nm)
0.193	(100)	0.003	46.24
0.275	(110)	0.004	34.67
0.339	(111)	0.006	23.11
0.394	(200)	0.007	19.81
0.443	(210)	0.009	15.41
0.489	(211)	0.005	27.74
0.573	(220)	0.010	13.87

5.2 SEM of BCZT and PVDF films

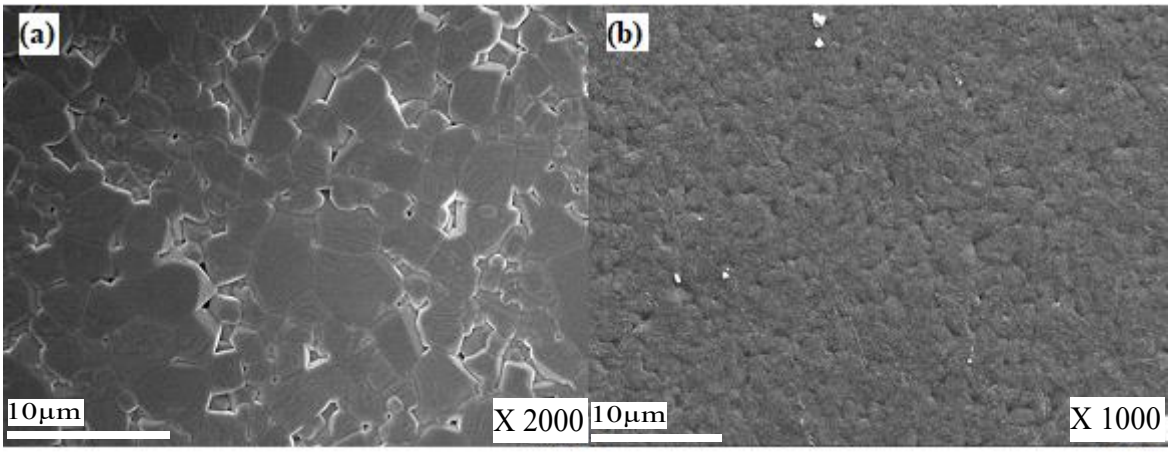

Figure 5.2 (a) SEM image of BCZT ceramic, **(b)** SEM image of PVDF thin film

Figure 5.2 (a) and (b) shows the SEM image of BCZT and PVDF films. From the images it is clear that clear that well defined grains are formed. The sample is free from any impurities. The nanoparticles are homogenously distributed which reveals that the synthesized sample is sintered well.

Chapter - 6

Conclusions and Future scopes

6.1 Conclusions

The subject of this dissertation is energy harvesting; that is extracting energy from nature-based sources such as air flow, vibrations and electromagnetic fields. In this case we focus on vibrations. The focus of this thesis is on the maximum power output can be obtained by harvesting energy from lead free piezoelectric material.

This thesis started with an introduction to various types of energy harvesting technologies followed by need of the environment-based energy harvesting technologies. For each energy source the relative advantages and disadvantages are outlined. We concluded that energy harvesting from piezoelectric transducers tends to result in higher power output. The detailed technological and historical contexts of piezoelectricity are introduced. It reviews the power enhancement of piezoelectric generators from first world war to present era, including the advances in design of the power generator and its applications. Along with piezoelectricity different types of piezoelectric materials are also discussed which includes the lead based and lead-free materials. After this the literature survey of lead-free materials (BCZT) and PVDF was done.

Following this; the experimental details of synthesis of BCZT and PVDF and the X-ray diffraction analysis along with SEM images of the sample is discussed. The sol-gel method is used to synthesize BCZT ceramic powder. The synthesized powder is calcined at 1000℃ and the average crystallite size of ~ 26nm is obtained. The SEM results confirmed the formation of well-defined grains.

6.2 Future scopes

- Piezoelectricity consists of enormous amount of applications in renewable and “GREEN ENERGY”.
- The power generated by this can be stored and can be used later.
- The lead-free piezoelectric materials like BCZT are non-toxic and have vast applications in our daily life.

References

1. Hajati, A. and S.-G. Kim, Ultra-wide bandwidth piezoelectric energy harvesting. Applied Physics Letters, 2011. **99**(8): p. 083105.
2. Calhoun, B.H., et al., Design considerations for ultra-low energy wireless microsensor nodes. IEEE Transactions on Computers, 2005. **54**(6): p. 727-740.
3. Roundy, S. and P.K. Wright, A piezoelectric vibration based generator for wireless electronics. Smart Materials and structures, 2004. **13**(5): p. 1131.
4. Roundy, S., P.K. Wright, and J. Rabaey, A study of low level vibrations as a power source for wireless sensor nodes. Computer communications, 2003. **26**(11): p. 1131-1144.
5. Freiman, S.W. and G.S. White, Intelligent ceramic materials: issues of brittle fracture. Journal of intelligent material systems and structures, 1995. **6**(1): p. 49-54.
6. Ballato, A. Piezoelectricity: history and new thrusts. in 1996 IEEE Ultrasonics Symposium. Proceedings. 1996. IEEE.
7. Katzir, S., The discovery of the piezoelectric effect, in THE BEGINNINGS OF PIEZOELECTRICITY. 2006, Springer. p. 15-64.
8. Oliveira, É.L., et al. Experimental aeroelastic investigation using piezoelectric transducers for modal parameters identification. 2015. SMART.
9. Unit cell of simple cubic lattice https://images.app.goo.gl/DNARgjuiqJ6Nge5AA taken on 2nd July 2020.
10. Categorisation of crystals belonging to the seven lattice systems https://images.app.goo.gl/Q61eCkhEaQB1XAUQ9 taken on 2nd July 2020.
11. A simple molecular model explaining the piezoelectric effect https://images.app.goo.gl/V5yEvv5XHPwVFWpVA taken on 2nd July 2020.
12. Jaffe, B., Piezoelectric ceramics. Vol. 3. 2012: Elsevier.
13. Rabinowitz, M.B., G.W. Wetherill, and J.D. Kopple, Kinetic analysis of lead metabolism in healthy humans. The Journal of Clinical Investigation, 1976. **58**(2): p. 260-270.
14. Takenaka, T., H. Nagata, and Y. Hiruma, Current developments and prospective of lead-free piezoelectric ceramics. Japanese Journal of Applied Physics, 2008. **47**(5S): p. 3787.

15. Ma, C., et al., Creation and destruction of morphotropic phase boundaries through electrical poling: a case study of lead-free $(Bi_{1/2}Na_{1/2})TiO_3-$ $BaTiO_3$ piezoelectrics. Physical review letters, 2012. **109**(10): p. 107602.
16. Saito, Y., et al., Lead-free piezoceramics. Nature, 2004. **432**(7013): p. 84-87.
17. Wang, X., et al., Giant piezoelectricity in potassium–sodium niobate lead-free ceramics. Journal of the American chemical society, 2014. **136**(7): p. 2905-2910.
18. Liu, W. and X. Ren, Large piezoelectric effect in Pb-free ceramics. Physical review letters, 2009. **103**(25): p. 257602.
19. Roberts, S., Dielectric and piezoelectric properties of barium titanate. Physical Review, 1947. **71**(12): p. 890.
20. Berlincourt, D. and H. Jaffe, Elastic and piezoelectric coefficients of single-crystal barium titanate. Physical Review, 1958. **111**(1): p. 143.
21. Keeble, D.S., et al., Revised structural phase diagram of $(Ba_{0.7}Ca_{0.3}TiO_3)$-$(BaZr_{0.2}Ti_{0.8}O_3)$. Applied Physics Letters, 2013. **102**(9): p. 092903.
22. Persano, L., et al., High performance piezoelectric devices based on aligned arrays of nanofibers of poly (vinylidenefluoride-co-trifluoroethylene). Nature communications, 2013. **4**(1): p. 1-10.
23. Sun, C., et al., PVDF microbelts for harvesting energy from respiration. Energy & Environmental Science, 2011. **4**(11): p. 4508-4512.
24. Gusarov, B., PVDF piezoelectric polymers: characterization and application to thermal energy harvesting. 2015.
25. Bera, B. and M.D. Sarkar, Piezoelectricity in PVDF and PVDF based piezoelectric nanogenerator: A concept. IOSR Journal of Applied Physics (IOSRJAP), 2017. **9**(3): p. 95-99.
26. Shrout, T.R. and S.J. Zhang, Lead-free piezoelectric ceramics: Alternatives for PZT? Journal of Electroceramics, 2007. **19**(1): p. 113-126.
27. Takenaka, T. and H. Nagata, Current status and prospects of lead-free piezoelectric ceramics. Journal of the European Ceramic Society, 2005. **25**(12): p. 2693-2700.
28. Bao, H., et al., A modified lead-free piezoelectric BZT–xBCT system with higher TC. Journal of Physics D: Applied Physics, 2010. **43**(46): p. 465401.
29. Xue, D., et al., Elastic, piezoelectric, and dielectric properties of $Ba(Zr_{0.2}Ti_{0.8})O_3$-$50(Ba_{0.7}Ca_{0.3})TiO_3$ Pb-free ceramic at the morphotropic phase boundary. Journal of Applied Physics, 2011. **109**(5): p. 054110.

30. Praveen, J.P., et al., Effect of poling process on piezoelectric properties of sol–gel derived BZT–BCT ceramics. Journal of the European Ceramic Society, 2015. **35**(6): p. 1785-1798.
31. Haertling, G.H., Ferroelectric ceramics: history and technology. Journal of the American Ceramic Society, 1999. **82**(4): p. 797-818.
32. Bai, Y., et al., (Ba,Ca)(Zr,Ti)O_3 lead-free piezoelectric ceramics—the critical role of processing on properties. Journal of the European Ceramic Society, 2015. **35**(13): p. 3445-3456.
33. Castkova, K., et al., Chemical Synthesis, Sintering and Piezoelectric Properties of $Ba_{0.85}Ca_{0.15}Zr_{0.1}Ti_{0.9}O_3$ Lead-Free Ceramics. Journal of the American Ceramic Society, 2015. **98**(8): p. 2373-2380.
34. Wang, Z., et al., Synthesis, structure, dielectric, piezoelectric, and energy storage performance of $(Ba_{0.85}Ca_{0.15})(Ti_{0.9}Zr_{0.1})O_3$ ceramics prepared by different methods. Journal of Materials Science: Materials in Electronics, 2016. **27**(5): p. 5047-5058.
35. Zhang, Y., et al., Dielectric and piezoelectric properties of porous lead-free $0.5Ba(Ca_{0.8}Zr_{0.2})O_3$-$0.5(Ba_{0.7}Ca_{0.3})TiO_3$ ceramics. Materials Research Bulletin, 2019. **112**: p. 426-431.
36. Parjansri, P., et al., Improvement in the electrical properties of BCZT Ceramics induced by self-seeds. Applied Physics A, 2019. **125**(6): p. 421.
37. Li, Z., A. Wu, and P. Vilarinho, Perovskite phase stabilization of Pb $(Zn_{1/3}Ta_{2/3})O_3$ ceramics induced by $PbTiO_3$ seeds. Chemistry of materials, 2004. **16**(4): p. 717-723.
38. Martins, P., A. Lopes, and S. Lanceros-Mendez, Electroactive phases of poly (vinylidene fluoride): Determination, processing and applications. Progress in polymer science, 2014. **39**(4): p. 683-706.
39. Mahale, B., D. Bodas, and S. Gangal, Study of $$\upbeta $$-phase development in spin-coated PVDF thick films. Bulletin of Materials Science, 2017. **40**(3): p. 569-575.
40. Patra, A., A. Pal, and S. Sen, Polyvinylpyrrolidone modified barium zirconate titanate/polyvinylidene fluoride nanocomposites as self-powered sensor. Ceramics International, 2018. **44**(10): p. 11196-11203.
41. Cullity, B.D., Elements of X-ray Diffraction. 1956: Addison-Wesley Publishing.
42. Schematic of Bragg's law from a crystal https://images.app.goo.gl/PMEWy6Cq3cK6RbCY9 taken on 2nd July 2020.
43. Experimental set-up of XRD https://images.app.goo.gl/nJHghefFARSKQiLdA taken on 2nd July 2020.

44. Seiler, H., Secondary electron emission in the scanning electron microscope. Journal of Applied Physics, 1983. **54**(11): p. R1-R18.
45. Experimental setup of SEM https://images.app.goo.gl/RwFec4NNnWHmHK6m7 taken on 2nd July 2020.

URKUND

Document Information

Analyzed document	Ankit Thesis.docx (D76167079)
Submitted	7/9/2020 4:05:00 AM
Submitted by	
Submitter email	dheeraj.kumar@thapar.edu
Similarity	7%
Analysis address	dheeraj.kumar.thapar@analysis.urkund.com

Sources included in the report

SA	**Mamta Shandilya.pdf** Document Mamta Shandilya.pdf (D29392376)	1
W	URL: https://www.researchgate.net/publication/323125051_Structural_and_electrical_prope ... Fetched: 6/6/2020 6:35:25 AM	4
SA	**sunil thesis.docx** Document sunil thesis.docx (D27614970)	1
W	URL: https://www.researchgate.net/publication/293045450_Synthesis_structure_dielectric_ ... Fetched: 4/8/2020 8:44:33 PM	1
W	URL: https://www.researchgate.net/publication/287374781_Effect_of_sintering_temperature ... Fetched: 6/16/2020 2:34:39 AM	2
W	URL: https://www.researchgate.net/publication/257955254_Revised_structural_phase_diagra ... Fetched: 4/24/2020 11:15:46 PM	1
W	URL: https://www.researchgate.net/publication/279213399_BaCaZrTiO3_lead-free_piezoelect ... Fetched: 4/8/2020 9:02:00 PM	2
W	URL: https://www.researchgate.net/publication/271605539_Effect_of_Ho_Doping_on_Piezoele ... Fetched: 6/6/2020 6:35:00 AM	2
W	URL: https://researchportal.bath.ac.uk/en/publications/dielectric-and-piezoelectric-pro ... Fetched: 7/9/2020 4:10:00 AM	2
W	URL: https://www.researchgate.net/publication/327216169_Dielectric_and_piezoelectric_pr ... Fetched: 7/9/2020 4:10:00 AM	4